

The $SU(N)$ Heisenberg model on the square lattice: a continuous- N quantum Monte Carlo study

K. S. D. Beach*

Department of Physics, University of Alberta, Edmonton, Alberta, Canada T6G 2G7

Fabien Alet, Matthieu Mambrini, and Sylvain Capponi

Université de Toulouse; UPS; Laboratoire de Physique Théorique (IRSAMC); F-31062 Toulouse, France and CNRS; LPT (IRSAMC); F-31062 Toulouse, France

(Dated: September 22, 2009)

A quantum phase transition is typically induced by tuning an external parameter that appears as a coupling constant in the Hamiltonian. Another route is to vary the global symmetry of the system, generalizing, e.g., $SU(2)$ to $SU(N)$. In that case, however, the discrete nature of the control parameter prevents one from identifying and characterizing the transition. We show how this limitation can be overcome for the $SU(N)$ Heisenberg model with the help of a singlet projector algorithm that can treat N continuously. On the square lattice, we find a direct, continuous phase transition between Néel-ordered and crystalline bond-ordered phases at $N_c = 4.57(5)$ with critical exponents $z = 1$ and $\beta/\nu = 0.81(3)$.

I. INTRODUCTION

The field of quantum magnetism encompasses a large variety of physical phenomena that are of current experimental and theoretical interest. These include competition between interactions (frustration), ordering in conventional or unconventional magnetic states, and the existence of fractionalized excitations. In two dimensions, where some of the most unusual physics occurs, there is a conspicuous absence of methods for studying the behaviour of quantum magnets with high precision. On the analytical side, neither the powerful methods devised for dimension $d = 1$ (bosonization, conformal field theory) nor the mean-field methods exact in high d are available. On the numerical side, simulations are difficult because of the enormous size of the Hilbert space and, for stochastic methods, because of the fatal “sign problem.”

One way to relax these strong methodological constraints is to decrease the role of quantum fluctuations. For instance, considering the classical limit of magnets with large spin S eases analytical studies. This limit, however, very often misses the important competition between the instabilities existing only at the quantum level. An alternative route—one that preserves the quantum fluctuations—is to enlarge the symmetry of the model, e.g., by extending the $SU(2)$ spin symmetry to $SU(N)$. This has proved very useful in the past, as the $N \rightarrow \infty$ limit often allows for an exact analytical treatment. Methods to study $1/N$ corrections are also available, although they cannot fully capture the exact details of what happens at finite N . The advantage of $SU(N)$ models over classical ones is that they naturally allow for quantum states of matter (such as valence bond solids) by construction, even if the off-diagonal elements of the Hamiltonian are suppressed in the large- N limit.

Using this technique, and building on previous work,¹ Read and Sachdev² have studied in detail the $SU(N)$ generalization of the Heisenberg Hamiltonian on the square

lattice. For sufficiently large N , the system spontaneously breaks lattice translation symmetry to form a valence bond crystal (VBC). For small N [including the standard $SU(2)$ model at $N = 2$], the ground-state is antiferromagnetically ordered. The details of the phase diagram and of the VBC depend on the representation of the generators of the $SU(N)$ algebra considered: for the case of square Young tableaux with n columns, a direct phase transition between the Néel and VBC states is predicted to occur at the (mean-field) value $N/n \sim 5.26$.

In a technical breakthrough, Kawashima and coworkers^{3,4,5} extended a quantum Monte Carlo (QMC) loop algorithm designed for $SU(2)$ models to the $SU(N)$ case (for all integer N and for all single-row Young tableaux). Studying the square lattice case with this exact numerical method, they found for $n = 1$ that the $N = 4$ model is Néel ordered, whereas the $N = 5$ model supports VBC order. This confirmed the analytical large- N predictions, but because of the discrete nature of the algorithm, these studies could not rule out an intermediate phase between $N = 4$ and 5. Even if this (possibly spin-liquid⁶) phase does not exist, it is impossible to obtain a precise value for the critical parameter N_c separating the two phases and to ascertain the nature of the phase transition at N_c .

In this paper, we describe a quantum Monte Carlo algorithm, formulated in the total singlet basis, that can treat the parameter N continuously (in the manner of analytical, large- N techniques). Applying this approach to the square-lattice $SU(N)$ Heisenberg model, we find that there is a direct transition occurring at $N_c = 4.57(5)$ between the Néel and VBC columnar phases. The transition is found to be second order, with critical exponents $z = 1$ and $\beta/\nu = 0.81(3)$. At the end of the paper we discuss the implications of finding a second-order quantum phase transition between states with incompatible symmetries and the possible connection to the deconfined quantum criticality (DQC) scenario.⁷

II. MODEL HAMILTONIAN

Our starting point is the $SU(N)$ generalization of the quantum Heisenberg model:

$$H = -J \sum_{\langle i,j \rangle} H_{ij} = \frac{J}{N} \sum_{\langle i,j \rangle} \sum_{\alpha,\beta=1}^N \mathcal{J}_\beta^\alpha(i) \mathcal{J}_\alpha^\beta(j). \quad (1)$$

Here, the exchange coupling $J = 1$ sets the energy scale, and $\langle i,j \rangle$ denotes nearest-neighbor sites i and j . The generators of the $SU(N)$ algebra, \mathcal{J}_β^α , satisfy the anti-commutation relation

$$[\mathcal{J}_\beta^\alpha(i), \mathcal{J}_{\beta'}^{\alpha'}(j)] = \delta_{ij} (\delta_{\alpha\beta'} \mathcal{J}_\beta^{\alpha'}(i) - \delta_{\alpha'\beta} \mathcal{J}_{\beta'}^\alpha(i)). \quad (2)$$

We consider the ‘‘quark-antiquark’’ model, taking the fundamental representation of the generator on one sublattice (a single-box Young tableau) and its conjugate ($N - 1$ boxes in one column) on the other. The fusion rule for the two representations is depicted graphically in Fig. 1(a).

If we describe the fundamental representation using a basis $|\alpha\rangle$ with $\alpha = 1, 2, \dots, N$, then the conjugate representation has states $|\bar{\alpha}\rangle$ that are fully antisymmetrized tensor products of the form

$$|\bar{\alpha}\rangle = \frac{1}{\sqrt{(N-1)!}} \sum_{\alpha_2, \dots, \alpha_N} \epsilon^{\alpha, \alpha_2, \dots, \alpha_N} |\alpha_2, \dots, \alpha_N\rangle. \quad (3)$$

An $SU(N)$ singlet formed between spins at sites i and j in opposite sublattices is the maximally entangled state

$$\begin{aligned} |\phi\rangle_{ij} &= \frac{1}{\sqrt{N}} \sum_{\alpha=1}^N |\alpha\rangle_i |\bar{\alpha}\rangle_j \\ &= \frac{1}{\sqrt{N!}} \sum_{\alpha_1, \dots, \alpha_N} \epsilon^{\alpha_1, \alpha_2, \dots, \alpha_N} |\alpha_1\rangle_i |\alpha_2, \dots, \alpha_N\rangle_j. \end{aligned} \quad (4)$$

Equation (1) can be understood as an operator that performs a local singlet projection $H_{ij} = -\frac{1}{N} \mathcal{J}_\beta^\alpha(i) \mathcal{J}_\alpha^\beta(j) = |\phi\rangle_{ij} \langle \phi|_{ij}$ across all links of the square lattice.

The $SU(N)$ Heisenberg model can alternatively be written as an $SU(2)$ system with spin $S = (N-1)/2$ moments interacting via higher-order exchange processes. An exact mapping connects the conventional $SU(2)$ spin operators to the $SU(N)$ generators as follows:

$$S^+ = \sum_{\alpha=1}^{N-1} \sqrt{\alpha(N-\alpha)} \mathcal{J}_\alpha^{\alpha+1}, \quad (5)$$

$$S^- = \sum_{\alpha=1}^{N-1} \sqrt{\alpha(N-\alpha)} \mathcal{J}_{\alpha+1}^\alpha, \quad (6)$$

$$S^z = \frac{1}{2} \sum_{\alpha=1}^N (N+1-2\alpha) \mathcal{J}_\alpha^\alpha. \quad (7)$$

The Hamiltonian can then be expressed in terms of

$$H_{ij} = \prod_{l=1}^{2S} \left[1 - 2 \left(\frac{S(S+1) + \mathbf{S}_i \cdot \mathbf{S}_j}{l(l+1)} \right) \right]. \quad (8)$$

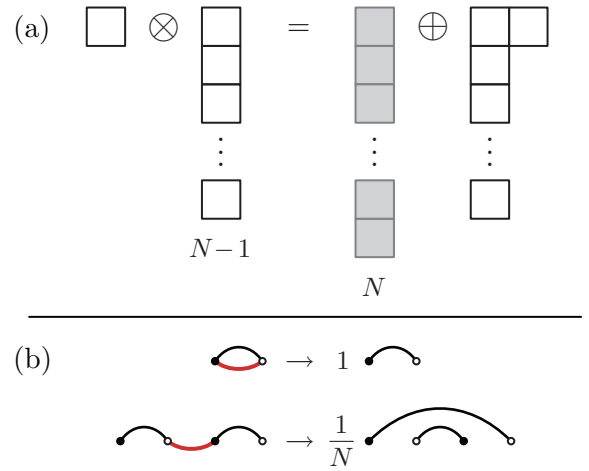


FIG. 1: (Color online) (a) An A-sublattice and a B-sublattice spin can pair to form a singlet, which corresponds to a column of zero (modulo N) boxes. (b) Update rules for the action of H_{ij} (red line) on VB singlet states (black bonds).

For instance, $H_{ij} = 1/4 - \mathbf{S}_i \cdot \mathbf{S}_j$ for $S = 1/2$ ($N = 2$); $H_{ij} = \frac{1}{3} [(\mathbf{S}_i \cdot \mathbf{S}_j)^2 - 1]$ for $S = 1$ ($N = 3$); etc. This was the starting point of previous finite-temperature QMC investigations of this model,^{3,4} where a path-integral technique was developed in the S_z basis of the spins.⁵ In this paper, we take a rather different route, using a $T = 0$ algorithm formulated in the $SU(2)$ total singlet basis of the spins S .

III. BOND BASIS

Consider the subspace formed by *bipartite valence bond* (VB) states⁸ in which two spins S in opposite sublattices form a VB by coupling pairwise in a singlet, formally given in the S_z basis by

$$|\phi\rangle_{ij} = \frac{1}{\sqrt{2S+1}} \sum_{m=-S}^S (-1)^{m-S} |m\rangle_i \otimes |-m\rangle_j \quad (9)$$

[cf. Eq. (4)]. For general S , this subspace does *not* span the full $SU(2)$ singlet manifold, but only the subspace of states that are also $SU(2S+1)$ symmetric.

For bipartite valence bonds, we can impose a VB orientation convention such that the overlap between any two states is positive. This basis is nonorthogonal, and the overlap between two VB states is

$$\langle v_1 | v_2 \rangle = (2S+1)^{N_l - N_v}, \quad (10)$$

where N_l is the number of *loops* formed by superimposing the two VB states $|v_1\rangle$ and $|v_2\rangle$, and N_v is the number of VBs in each state (or, equivalently, half the number of lattice sites). This is a simple generalization of the well-known overlap rule for $S = 1/2$.

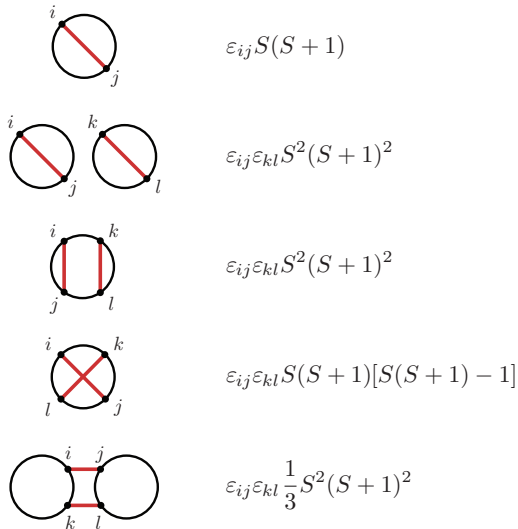


FIG. 2: (Color online) Loop diagrams contributing to two- and four-spin correlators $[\mathbf{S}_i \cdot \mathbf{S}_j$ and $(\mathbf{S}_i \cdot \mathbf{S}_j)(\mathbf{S}_k \cdot \mathbf{S}_l)$, respectively] and their contributions. These overlap loops (schematically circular here) are obtained by superimposing the VB configurations $|v_1\rangle$ and $|v_2\rangle$. The straight (red) lines link the corresponding sites of the correlation function. Only diagrams with nonvanishing contributions are displayed.

The Perron-Frobenius theorem tells us that on a bipartite, finite lattice the $SU(N)$ symmetric Hamiltonian (1) admits a unique ground state. This state is an $SU(N)$ singlet, which can be expressed in the bipartite VB basis.

The operator H_{ij} obeys the rules $H_{ij}|\phi\rangle_{ij} = |\phi\rangle_{ij}$ and $H_{ij}|\phi\rangle_{il}|\phi\rangle_{kj} = \frac{1}{N}|\phi\rangle_{ij}|\phi\rangle_{kl}$. As a consequence, the action of H_{ij} on VB states is extremely simple⁹ and consists of the bond rearrangements depicted in Fig. 1(b). We exploit this fact to simulate the $SU(N)$ model, noting that the VB projector QMC (Ref. 10) developed for $S = 1/2$ works with *precisely such update rules*. For the sake of completeness, we describe this method (emphasizing the few details that differ) in Sec. IV.

What remains is to determine how to compute observables. It is well-known in the $S = 1/2$ case that most observables can be written in terms of estimators based on the overlap loops.⁸ For instance, the spin correlator $\langle v_1 | \mathbf{S}_i \cdot \mathbf{S}_j | v_2 \rangle / \langle v_1 | v_2 \rangle = (3/4)\epsilon_{ij}$ if spins i and j belong to the same loop, 0 otherwise. Here $\epsilon_{ij} = 1$ if i and j are on the same sublattice, -1 otherwise. We have generalized these rules for the spin S case, and the resulting nonvanishing loop diagrams are given in Fig. 2, alongside the value of their contribution.

We now make our key observation: since the update rules, the Monte Carlo weights, and the estimators have analytical expressions in N (or S , via $N = 2S + 1$), simulations can be performed for *arbitrary, continuous values of N* . Formally, this can be understood as an analytic continuation from integer to real N . This is a great advantage over other QMC techniques,⁵ which are restricted to half-integer and integer S . Large- N analyt-

ical techniques² can also treat continuous values of N , but our numerical technique allows for an *exact* treatment of the Hamiltonian, in contrast to the mean-field approximation inherent to the large- N approach.

IV. NUMERICAL METHOD

A. Quantum Monte Carlo algorithm

We employ an efficient Monte Carlo algorithm that is an extension of the VB projector scheme introduced by Sandvik.¹⁰ The idea is to sample the ground state via the power method by applying $(-H)^M$ (for fixed M sufficiently large) to an arbitrary valence bond trial state:

$$|\psi_0\rangle = \lim_{M \rightarrow \infty} (-H)^M |\varphi_T\rangle. \quad (11)$$

For the purpose of sketching out the algorithm, it is convenient to rewrite Eq. (1) in a form that explicitly indexes the bonds that are acted upon:

$$-H/J = \sum_{\langle ij \rangle} H_{ij} = \sum_b H_b. \quad (12)$$

We make the equivalence $H_b = H_{i(b),j(b)}$, where b labels all the nearest-neighbour bonds on the square lattice. We now expand the powers of the Hamiltonian as

$$(-H)^M = \left(\sum_b H_b \right)^M = \sum_{\{b_1, b_2, \dots, b_M\}} \prod_{k=1}^M H_{b_k}. \quad (13)$$

Each sequence $\{b_1, b_2, \dots, b_M\}$ corresponds to the process in which $|\varphi_T\rangle$ is acted on by local singlet projectors to give the propagated VB state $|\varphi_M\rangle$:

$$|\varphi_M\rangle = H_{b_M} \dots H_{b_2} H_{b_1} |\varphi_T\rangle. \quad (14)$$

The sum over all possible sequences in Eq. (13) is evaluated stochastically. For the $SU(N)$ model, the weight of each sequence is simply the product of the $1/N$ factors (with $N = 2$ for $S = 1/2$) that appear as a result of the bond rearrangements [see Fig. 1(b)] induced by the H_b 's. The most basic Monte Carlo move then consists of replacing a few H_b 's at random. Such changes are accepted or rejected depending on the ratio of the weight before and after the move.¹⁰

To compute observables, two such sequences are generated with an additional factor in the sampling weight corresponding to the overlap of the two propagated states. For the $SU(N)$ model, this is computed according to Eq. (10). The observables can then be measured using the loop estimators of Fig. 2 (see Sec. IV B).

The spin gap Δ_s , the energy difference between the first triplet excited state and the singlet ground state, can be computed using the same triplet propagation technique introduced for the $S = 1/2$ case.^{8,10} Working with

a single propagation sequence, we reinterpret the initial VB trial state as containing one triplet bond; the only difference in the propagation rules is that the triplet is annihilated by H_b when acted on directly [i.e., the coefficient 1 in the first rule of Fig. 1(b) is replaced by 0]. Looking at the statistics of the states that are not annihilated during the full propagation, one can easily compute the spin gap Δ_s . We refer the reader to Refs. 8 and 10 for more details.

To accelerate the convergence of the algorithm with respect to M , it is useful to sample a valence bond trial state that is a superposition of all valence bond configurations v with amplitude $\varphi_T(v)$:

$$|\varphi_T\rangle = \sum_v \varphi_T(v)|v\rangle. \quad (15)$$

There is no restriction on the trial state other than that $\varphi_T(v)$ be real and nonnegative and that ratios $\varphi_T(v_2)/\varphi_T(v_1)$ be easy to compute for small changes in configuration $v_1 \rightarrow v_2$. In this work, we make use of a simple RVB trial state¹¹ in which the weight $\varphi_T(v) = \prod_{[i,j] \in v} h_{ij}$ is a product of individual bond amplitudes $h_{ij} = 1/r_{ij}^p$ that fall off algebraically as a function of the bond length. The trial state is thus characterized by a single exponent p , which is a free parameter in our simulations. To ensure that our results are fully converged (i.e., that M has been chosen sufficiently large) and do not show any residual dependence on the choice of p , we have carried out the ground state projection starting from four different RVB trial states (two magnetically ordered and two disordered) corresponding to $p = 2.7, 3.0, 3.5, \text{ and } 5.0$, and have checked that all observables converge to the same values.

We should point out that the updates are simple and sign-problem-free only because H_{ij} , appearing in Eqs. (1) and (8), is a pure, local-singlet projector. Our algorithm does not apply to general spin- S Hamiltonians. In any case, the bipartite VB states do not form a basis for the singlet sector of general spin- S models.

B. Calculation of observables

The quantities of interest at the transition are the staggered magnetization

$$\mathbf{M} = \frac{1}{L^2} \sum_{\mathbf{r}} (-1)^{r_x+r_y} \mathbf{S}_{\mathbf{r}}, \quad (16)$$

its Binder cumulant

$$U = 1 - \frac{3\langle \mathbf{M}^4 \rangle}{5\langle \mathbf{M}^2 \rangle^2}, \quad (17)$$

and the dimer order parameter $\mathbf{D} = (D_x, D_y)$, whose two components

$$D_a = \frac{1}{L^2} \sum_{\mathbf{r}} (-1)^{r_a} \mathbf{S}_{\mathbf{r}} \cdot \mathbf{S}_{\mathbf{r}+\hat{\mathbf{e}}_a} \quad (a = x, y) \quad (18)$$

are directed along the square lattice vectors $\hat{\mathbf{e}}_x$ and $\hat{\mathbf{e}}_y$.

The measurements $\langle \mathbf{M}^2 \rangle$, U , and $\langle \mathbf{D}^2 \rangle$ are carried out using the two- and four-point rules shown in Fig. 2. For instance, using the same techniques as in Ref. 8, we obtain the following estimators:

$$\frac{\langle \varphi_M | \mathbf{M}^2 | \varphi'_M \rangle}{\langle \varphi_M | \varphi'_M \rangle} = S(S+1) \sum_{\alpha} L_{\alpha}^2 \quad (19)$$

and

$$\begin{aligned} \frac{\langle \varphi_M | \mathbf{M}^4 | \varphi'_M \rangle}{\langle \varphi_M | \varphi'_M \rangle} &= -\frac{1}{3} [S(S+1) + 2S^2(S+1)^2] \sum_{\alpha} L_{\alpha}^4 \\ &+ \frac{4}{3} S(S+1) \sum_{\alpha} L_{\alpha}^2 \\ &+ \frac{5}{3} S^2(S+1)^2 \left(\sum_{\alpha} L_{\alpha}^2 \right)^2, \end{aligned} \quad (20)$$

where the sum on α runs over all loops formed by the overlap $\langle \varphi_M | \varphi'_M \rangle$ of the two propagated states, and L_{α} is the size of a given loop.

V. RESULTS

We proceed by presenting our results for the square lattice $SU(N)$ model. Figure 3 shows the square of the staggered magnetization and its Binder cumulant. It is apparent that in the thermodynamic limit a dome of antiferromagnetic order survives for $1 < N < N_c$ with N_c between 4 and 5. The Binder cumulant U vanishes on the large- N side of the transition and appears to have a crossing point at $N \approx 4.3$, which drifts rightward as L increases. We do not have data on sufficiently large systems to ascertain that the crossing is stable and can be unambiguously identified as the critical point. As we will see, a finite-size scaling analysis provides a better estimate of N_c .

The destruction of the Néel order is driven by the gradual elimination of singlet pairs that are correlated over long distances. In the large- N phase, the singlets are predominantly short-ranged and form domains of columnar ordering (see Fig. 4). On small lattices, these ordered domains are weak and they are almost equally distributed among the four degenerate configurations. This can be seen in the ring-like structure of the probability distribution $P(D_x, D_y)$, shown in Fig. 5, that appears for $N > N_c$. Previous work^{3,4} established the existence of VBC order for $N \geq 5$, but could not determine whether it was of columnar [$\langle \mathbf{D} \rangle \sim (0, \pm D), (\pm D, 0)$] or plaquette [$\langle \mathbf{D} \rangle \sim (\pm D, \pm D)$] symmetry. Our results suggest the former. There does not appear to be a true $U(1)$ degeneracy, as suggested in Ref. 3. Instead, it seems that there is an additional length scale ξ_{VBC} much larger than the spin correlation length ξ . For $\xi < L < \xi_{\text{VBC}}$, there is merely an effective $U(1)$ degeneracy.

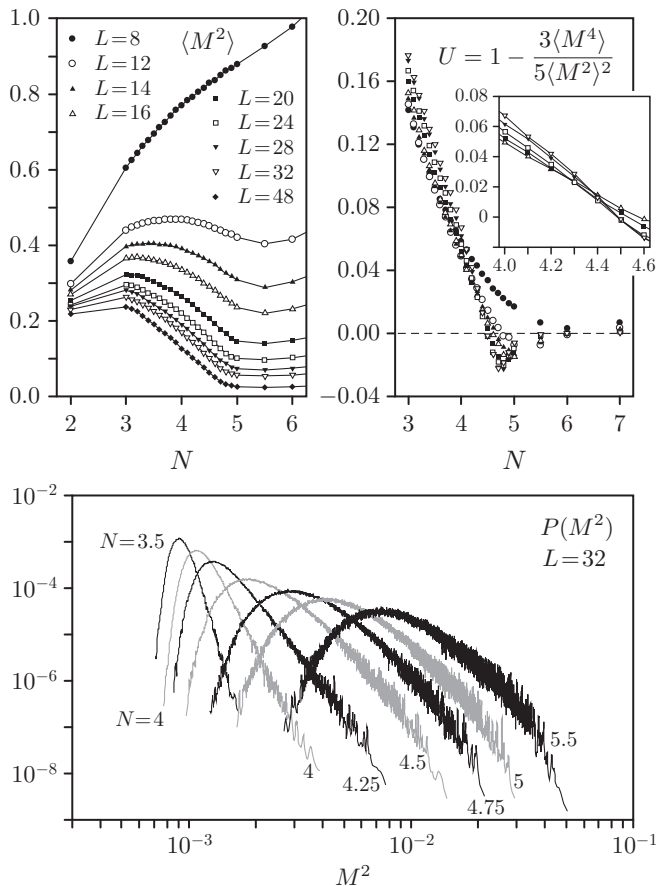


FIG. 3: (Top-left panel) Square of the staggered magnetization $\mathbf{M} = \frac{1}{L^2} \sum_{\mathbf{r}} (-1)^{r_x+r_y} \mathbf{S}_{\mathbf{r}}$ as a function of N for systems up to linear size $L = 48$ (lines are guides to the eyes). (Top-right panel) The Binder cumulant U measures the kurtosis of the staggered magnetization with respect to a purely Gaussian distribution. It vanishes in the limit $L \rightarrow \infty$ in the absence of antiferromagnetic order. (Bottom panel) A histogram of the magnetic observable is shown for values of N spanning the transition. The distribution has a single peak.

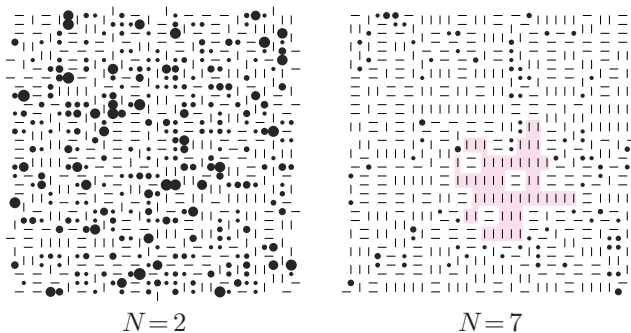


FIG. 4: (Color online) Snapshots of typical VB configurations for a system of size $L = 32$. Short, nearest-neighbour bonds are drawn with a line; long bonds are indicated by circles (whose area is proportional to bond length) at their end points. For $N < N_c$, many long bonds stretch across the system. For $N > N_c$, short bonds dominate. The shaded (pink) area marks a crystal domain with columnar bond order.

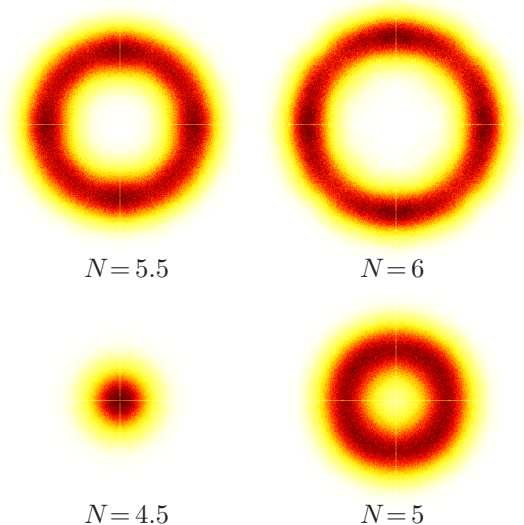


FIG. 5: (Color online) Density plots of histograms $P(D_x, D_y)$ of the x - and y - components of the dimer order parameter ($L = 32$). On the magnetic side of the transition (e.g., $N = 4.5 < N_c$), the distribution is characterized by a central peak. On the VBC side, the distribution is ring-like but develops additional weight along the main axes as N is increased.

A finite-size scaling analysis of the magnetization and dimer order parameters suggests a continuous transition defined by a single critical value N_c and a single set of critical exponents (see Fig. 6). The data are not sufficiently sensitive to fix the exponent ν precisely, and the unusual behaviour of the Binder cumulant—its negative region and strong subleading corrections—makes it unreliable for obtaining an independent estimate of ν . Reasonable fits seem to be achievable for a range of values $0.75 \lesssim \nu \lesssim 1$. On the other hand, the ratio β/ν is relatively stable. Repeating our fitting procedure for M^2 and D^2 independently with 3000 bootstrap samples, we conclude that both quantities vanish simultaneously and continuously at $N_c = 4.57(5)$ with $\beta/\nu = 0.81(3)$. Note that the anomalous dimension $\eta = 2\beta/\nu - 1 = 0.63(4)$ is at least an order of magnitude larger than what would be expected from either the three-dimensional $O(3)$ or \mathbb{Z}_4 universality classes.

In Fig. 7, we plot the spin gap as a function of $1/L$ in the region $4 \leq N \leq 5$. For N large enough, the data converges to a nonzero value in the thermodynamic limit. On the other hand, for the smallest N , the gap clearly vanishes. A linear extrapolation in $1/L$ (dashed lines in Fig. 7) reveals that the gap closes at $N \approx 4.6$, in good agreement with the value $N_c = 4.57(5)$ derived from the order parameters. An unconstrained power-law fit yields a slope $1.02(10)$, confirming that the dynamical critical exponent of the phase transition is $z = 1$.

As is the case for any finite-lattice simulation, we cannot completely rule out an extremely weak first-order transition. Nonetheless, we have taken great care to ex-

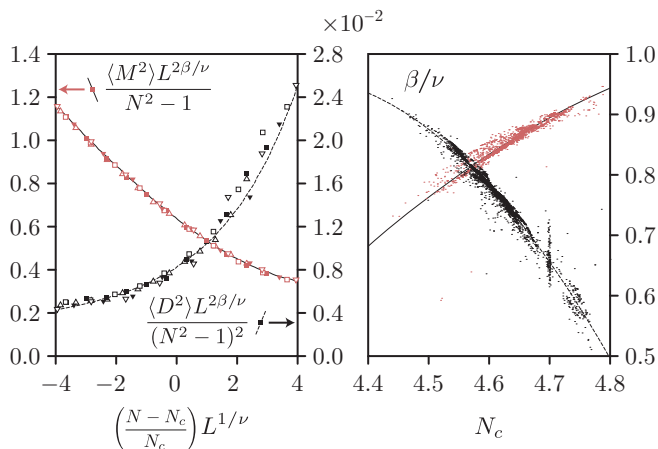


FIG. 6: (Color online) Simultaneous data collapse of the Néel and dimer correlations can be achieved with a single set of critical exponents. The left panel shows the QMC measurements plotted in rescaled coordinates with the values $\nu = 0.88$, $\beta = 0.71$, and $N_c = 4.57(5)$. Other values of $\beta/\nu \sim 0.8$ produce good data collapse. The right panel shows bootstrapped results of β/ν versus N_c when fits of M^2 and D^2 are performed independently. A single critical point corresponds to the crossing $\beta/\nu = 0.81(3)$ and $N_c = 4.57(5)$.

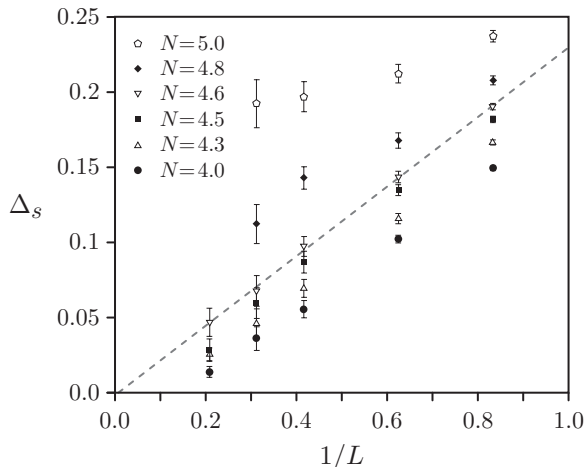


FIG. 7: The spin gap Δ_s versus the inverse linear size $1/L$ close to the critical point. The dashed line indicates a linear fit for $N = 4.6$ that extrapolates very close to 0 in the thermodynamic limit.

amine the transition for signs of first-order character and have concluded that it is almost certainly continuous. We have generated energy and order parameter histograms with extremely good statistics close to the transition and have found no evidence of a bimodal character. See, e.g., the distribution of the staggered magnetization, shown in the bottom panel of Fig. 3, which is single-peaked and evolves smoothly across the transition.

One point of concern was that the Binder cumulant has a small region around the transition where it drops below zero. This is sometimes a signature of a first-order transi-

tion or of a distribution with a complicated multi-peaked structure. The histograms discussed above rule out the latter: the negative U seems merely to correspond to a region in which the distribution of the magnetic order parameter is super-Gaussian (excess kurtosis). Another important observation relates to how the negative region evolves with system size. For first-order phase transitions, one typically observes very large negative values of the Binder cumulant that *increase* in magnitude with the system size. This has been explained phenomenologically by Vollmayr et al.¹² For the transition observed here, the opposite is true: not only are the values only slightly negative, but a careful examination shows that the height of the dip begins to saturate starting around $L = 28$. In addition to the depth of the negative region being bounded, its width also vanishes in the thermodynamic limit. Finally, it is also worth pointing out that the behaviour of the $SU(N)$ transition reported in this work bears little resemblance to the transition in models whose Néel-VBS transition is known to be first-order (e.g., Ref. 13), which is marked by strong hysteresis effects even at small lattice sizes. These observations suggest to us that the behaviour is only a finite-size effect.

VI. CONCLUSION

In conclusion, we have introduced an algorithm to simulate Heisenberg $SU(N)$ models (for the representation with a single row and column on one sublattice and its conjugate on the other) on any bipartite lattice. It is formulated in the total singlet sector and allows for efficient computation with arbitrary, continuous values of N . For the square-lattice model, we find a second-order phase transition between a Néel and VBC columnar state at $N_c = 4.57(5)$. Constructing a Ginzburg-Landau theory for this phase transition is not simple from the symmetry point of view, as the external parameter N of the $SU(N)$ symmetry is tuned artificially to unphysical values in our numerics. Naively, the ingredients seem similar to those encountered in DQC points^{7,14}: a continuous Néel-VBC transition, driven by an external parameter that favors short VBs of the VBC over the long VBs needed for magnetic ordering. Strictly speaking, the arguments of Ref. 7 do not apply here, since they rely heavily on Berry phase effects specific to $S = 1/2$. Hence, our results are not directly related to those of Refs. 7 and 14. The large- N techniques of Ref. 2 do predict a continuous transition from Néel order to disorder, but the ground state degeneracy can only be computed for integer N . We hope that our numerical results for the critical exponents encourage others to pursue extended analytical calculations: the only available estimates of exponents¹⁵ are for representations with $n \gg 1$ and do not go beyond order $1/N$.

Finally, we note that the algorithm presented here can be applied with minor modifications to the case of one-dimensional Heisenberg models with another generalized symmetry, namely $SU(2)_k$. This opens the door to the

numerical study of topological quantum liquids, as found in Ref. 16.

During the completion of this work, a more efficient algorithm for the $N = 2$ case was proposed by Sandvik and Evertz.¹⁷ This algorithm performs nonlocal moves by flipping spins around the loops in a mixed spin-VB representation of the projection. It is straightforward to generalize this algorithm to the $SU(N)$ case for integer N , as has been done in Ref. 18. One of us¹⁹ has recently shown that an algorithm for real N can be constructed using a loop representation of the $SU(N)$ model matrix

elements similar to the one presented in Ref. 20. Early results obtained with this algorithm are in agreement with those presented in this work.

We thank K. Harada and N. Kawashima for fruitful exchanges. Some calculations were performed using the ALPS libraries (Ref. 21). We thank IDRIS and CALMIP for allocation of CPU time. Support from the Procope (Egide), the French ANR program under Grant No. ANR-08-JCJC-0056-01 (FA, MM, and SC) and from the Alexander von Humboldt foundation (KSDB) is acknowledged.

-
- * Electronic address: kbeach@phys.ualberta.ca
- ¹ A. Auerbach and D. P. Arovas, Phys. Rev. Lett. **61**, 617 (1988); D. P. Arovas and A. Auerbach, Phys. Rev. B **38**, 316 (1988).
 - ² N. Read and S. Sachdev, Phys. Rev. Lett. **62**, 1694 (1989); Nucl. Phys. **B316**, 609 (1989); Phys. Rev. B **42**, 4568 (1990).
 - ³ N. Kawashima and Y. Tanabe, Phys. Rev. Lett. **98**, 057202 (2007).
 - ⁴ K. Harada, N. Kawashima and M. Troyer, Phys. Rev. Lett. **90**, 117203 (2003).
 - ⁵ N. Kawashima and K. Harada, J. Phys. Soc. Jap. **73**, 1379 (2004).
 - ⁶ G. Santoro, S. Sorella, L. Guidoni, A. Parola, and E. Tosatti, Phys. Rev. Lett. **83**, 3065 (1999).
 - ⁷ T. Senthil, L. Balents, S. Sachdev, A. Vishwanath, and M. P. A. Fisher, Science **303**, 1490 (2004); Phys. Rev. B **70**, 144407 (2004); J. Phys. Soc. Jpn. Suppl. **74**, 1 (2005).
 - ⁸ K. S. D. Beach and A. W. Sandvik, Nucl. Phys. B **750**, 142 (2006).
 - ⁹ I. Affleck, J. Phys.: Condens. Matter **2**, 405 (1990).
 - ¹⁰ A. W. Sandvik, Phys. Rev. Lett. **95**, 207203 (2005).
 - ¹¹ S. Liang, B. Douçot, and P. W. Anderson, Phys. Rev. Lett. **61**, 365 (1988).
 - ¹² K. Vollmayr, J. D. Reger, M. Scheucher, and K. Binder, Z. Phys. B **91**, 113 (1993).
 - ¹³ K. S. D. Beach and A. W. Sandvik, Phys. Rev. Lett. **99**, 047202 (2007).
 - ¹⁴ O. I. Motrunich and A. Vishwanath, Phys. Rev. B **70**, 075104 (2004); A. W. Sandvik, Phys. Rev. Lett. **98**, 227202 (2007); R. G. Melko and R. K. Kaul, Phys. Rev. Lett. **100**, 017203 (2008); F.-J. Jiang, M. Nyfeler, S. Chandrasekharan, and U.-J. Wiese, J. Stat. Mech. P02009 (2008)
 - ¹⁵ B. I. Halperin, T. C. Lubensky, and S.-K. Ma, Phys. Rev. Lett. **32**, 292 (1974); V. Y. Irkhin, A. A. Katanin, and M. I. Katsnelson, Phys. Rev. B **54**, 11953 (1996).
 - ¹⁶ A. Feiguin, S. Trebst, A. W. W. Ludwig, M. Troyer, A. Kitaev, Z. Wang, and M. H. Freedman, Phys. Rev. Lett. **98**, 160409 (2007).
 - ¹⁷ A. W. Sandvik and H. G. Evertz, arXiv:0807.0682.
 - ¹⁸ J. Lou, A. W. Sandvik, N. Kawashima, arXiv:0908.0740.
 - ¹⁹ K. S. D. Beach, (unpublished).
 - ²⁰ M. Aizenman and B. Nachtergaele, Comm. Math. Phys. **164**, 17 (1994).
 - ²¹ F. Albuquerque, F. Alet, P. Corboz, P. Dayal, A. Feiguin, S. Fuchs, L. Gamper, E. Gull, S. Grtler, A. Honecker, R. Igarashi, M. Körner, A. Kozhevnikov, A. Läuchli, S. R. Manmana, M. Matsumoto, I. P. McCulloch, F. Michel, R. M. Noack, G. Pawłowski, L. Pollet, T. Pruschke, U. Schollw ock, S. Todo, S. Trebst, and M. Troyer, J. Magn. Mater. **310**, 1187 (2007); M. Troyer, B. Ammon and E. Heeb, Lect. Notes Comput. Sci., **1505**, 191 (1998); see <http://alps.comp-phys.org>.